Journal of Applied Polymer Science

Structure Evolution During Uniaxial Tensile Deformation of High Density Polyethylene Before and After Irradiation by 1 MeV Electrons

Erming Rui,[1] Jianqun Yang,[1] Xingji Li,[1] Chaoming Liu,[1] Feng Tian,[2] Feng Gao,[3] Xiuhong Li,[2] Hongbin Geng[1]

[1]School of Materials Science and Engineering, Harbin Institute of Technology, Harbin 150001, China
[2]Shanghai Institute of Applied Physics, Chinese Academy of Sciences, Shanghai 201203, China
[3]National Center for Nanoscience and Technology, Chinese Academy of Sciences, Beijing 100190, China
Correspondence to: X. Li (E - mail: lxj0218@hit.edu.cn)

ABSTRACT: The structural evolution of high density polyethylene (HDPE) during uniaxial tensile deformation, before and after irradiation by 1 MeV electrons, is *in situ* studied by synchrotron small angle X-ray scattering (SAXS) and wide angle X-ray diffraction (WAXD). Both the pristine and the irradiated HDPE exhibit three regions of deformation behavior. It is shown that the deformation in the first region is in accord with the change in long period of the lamellar structure. In the following two regions, both the strain-induced melting and strain-induced crystallization could occur. The tensile stress decreases with strain in the second region due to the dominant melting effect. In the third region, the synergistic effect of the melting and crystallization results in stress leveling off first, and then the tensile stress increases again because the crystallization effect becomes dominant at higher strains. For the irradiated HDPE, the irradiation-induced crosslinking network slows down the deformation process. Compared to the pristine one, all the tensile stress is rather higher at a given strain for the irradiated HDPE. © 2013 Wiley Periodicals, Inc. J. Appl. Polym. Sci. **2014**, *131*, 40269.

KEYWORDS: structure–property relations; irradiation; crosslinking; X-ray

Received 2 September 2013; accepted 7 December 2013
DOI: 10.1002/app.40269

INTRODUCTION

Polyethylene (PE) is a typical polymer that consists of organic molecules to be polymerized into very long chains. The high molecular weight and molecular entanglement of PE give rise to its unique properties, such as the good toughness, high resilience, high strength-to-weight ratio and the ability to be moulded. Because of these valuable properties, PE is widely used in space applications, such as thermal blankets, circuit boards and insulation films.[1]

It is of importance to evaluate the sensitivity of PE to space radiations, such as electrons, protons and heavy ions.[2,3] When exposed to a radiation environment, PE favors crosslinking, primarily in the noncrystalline phase and along the lamellar amorphous interphase.[4,5] The crosslinking caused by radiation can change the properties of PE,[6,7] and the change in properties could affect the spacecraft reliability. For example, when used as a structural material, it needs to bear applied loads, and the structural change of PE caused by space radiation would influence its mechanical properties directly. Therefore, the deformation behavior and structure change mechanisms of the irradiated PE are worth deep studying.

The changes in structure of PE during deformation have been examined by the electron microscopy, infrared spectroscopy, pulsed nuclear magnetic resonance and laser profilometry for many years.[8–15] Also, the deformation mechanisms of the crosslinked PE have been investigated by scanning electron microscopy, and transmission electron microscopy.[16,17] Compared to the above traditional methods, the synchrotron radiation, discovered in 1960s, is of benefit to reveal the deformation mechanisms of polymers *in situ*. It was first used to study the crystallization and melting behavior of PE in 1988.[18,19] and to study the deformation behavior of PE in 1990.[20] From then on, synchrotron radiation has been extensively used to study the deformation mechanisms of PE.[21–30] However, up to now, there are few works to investigate the *in situ* deformation behavior of the irradiated PE by means of synchrotron radiation. It is important to make a scrutiny into the change in structure of the irradiated PE during deformation using synchrotron radiation, for the results could richen scientific implication for the deformation mechanisms of polymers.

The synchrotron radiation technique with a combined small angle X-ray scattering (SAXS) and wide angle X-ray diffraction (WAXD) setup can provide detailed information on both the

molecular and supramolecular length scales. In this article, both the SAXS and WAXD are used to characterize the structure evolution during uniaxial tensile deformation for the pristine and the irradiated high density polyethylene (HDPE). The effect of radiation on the deformation mechanisms of HDPE is discussed, and the deformation models for both the unirradiated and the irradiated HDPE are proposed.

MATERIALS AND METHODS

Materials Preparation

HDPE with an averaged molecular weight (weight average molecular weight) of 300,000 g mole^{-1} was provide by National center for Nanoscience and Technology of China. The HDPE was prepared using a screw extruder at a barrel temperature of 140°C, and the screw is 80 rpm. The thickness of samples is 0.5 mm, which are compressed and moulded under 25 MPa at 150°C for 5 min warming up and 5 min pressure-keeping, and following by a natural cooling down.

Samples, placed between two glasses with smooth surface, were put into a vacuum oven under 95°C for 30 min after moulding. Then, the samples were cooled down to room temperature with a speed of 0.1°C min^{-1}. To release electric charge on the surface and inside samples, a "short circuit" treatment was done. The samples were placed between two mirror surface copperplates connected by wires, and were put into a vacuum oven under 80°C for 24 h. Then the samples were cooled down to room temperature under 0.1°C min^{-1}.

The electron irradiation test was performed using an accelerator in Harbin Institute of Technology, China. The electron energy was set at 1 MeV, and the fluence at 1.2×10^{14} cm^{-2}.

Tensile Testing

The length, width and thickness for the dog-bone-shaped samples are 10, 4, and 0.5 mm, respectively. Uniaxial tensile deformation was performed with a home-made tensile apparatus with a speed of 1.16 μm s^{-1} at room temperature. The initial strain rate is 0.007 min^{-1}. As a result of extension, the strain rate varies throughout the drawing but is always no more than 0.007 min^{-1}. The stress and strain mentioned through the article are all engineering stress and engineering strain, respectively. The tensile testing was performed to a strain of 100%, less than the tensile fracture strain. The testing is focused on revealing lower deformation behavior of the samples.

SAXS and WAXD Measurements

The SAXS and WAXD were used to *in situ* characterized the structure evolution of HDPE samples during tensile deformation. The SAXS and WAXD tests were performed on beamline BL16B1 of the Shanghai Synchrotron Radiation Facility (SSRF). The incident X-ray wavelength λ is 0.124 nm, and the sample to detector distances are 5.1 m (SAXS) and 0.1 m (WAXD). The SAXS and WAXD images were taken immediately after the required strain values had been reached during the deformation process. The intensity profiles were recorded with a two-dimensional imaging plate at room temperature. All the X-ray scattering data were corrected for the background and air scattering, the beam fluctuations and sample thickness variations.

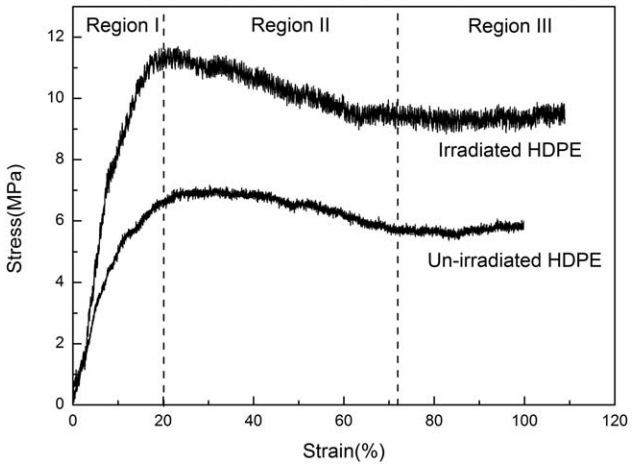

Figure 1. Engineering uniaxial stress–strain curves for the pristine and the irradiated HDPE.

RESULTS AND DISCUSSION

Stress–Strain Curves

Figure 1 shows the engineering uniaxial stress-strain curves for the pristine and the irradiated HDPE. It can be seen that the stress–strain curves for both the samples show three characteristic regions, similar to other research.[31] In the initial region (region I), corresponding to the strains from 0 to 20%, the stress increases with increasing strain from the elastic region up to the ultimate point, showing an obvious strain-hardening effect. It is noticed that a linear relationship between stress and strain exhibits before the strain of 10%, while a nonlinear relationship develops during the strains from 10 to 20% for the pristine sample and a second linear relationship with different slope develops during the strains from 10 to 20% for the irradiated sample. In the second region (region II), corresponding to the strains from 20 to 72%, the stress decreases with strain gradually, demonstrating a character of strain-softening. In the third region (region III), corresponding to the strains from 72% to more than 100%, the stress tends to level off and then to increase with strain again. This phenomenon indicates that a secondary strain-hardening occurs. It is illustrated that the deformation behavior during the strains from 72 to 100% could represent the third stage deformation feature for the HDPE samples, although the strain of 100% does not reach the tensile fracture strain. In addition, it is of interest to note that the stress values of the irradiated HDPE are about two times higher than those of the unirradiated one. Especially, the strain-hardening rate in the region I for the irradiated HDPE is relatively higher than that for the unirradiated one.

SAXS Analysis

Figures 2 and 3 give the *in situ* SAXS patterns for the pristine and the irradiated HDPE during uniaxial tensile deformation, respectively. For both the unirradiated and the irradiated HDPE, isotropic scattering patterns are observed when the deformation is zero, as shown in Figures 2(a) and 3(a). This implies that the molecular structure has no preferential orientation and is comprised of stacks of randomly oriented chain-folded lamellae of amorphous chains.[31] In the region I,

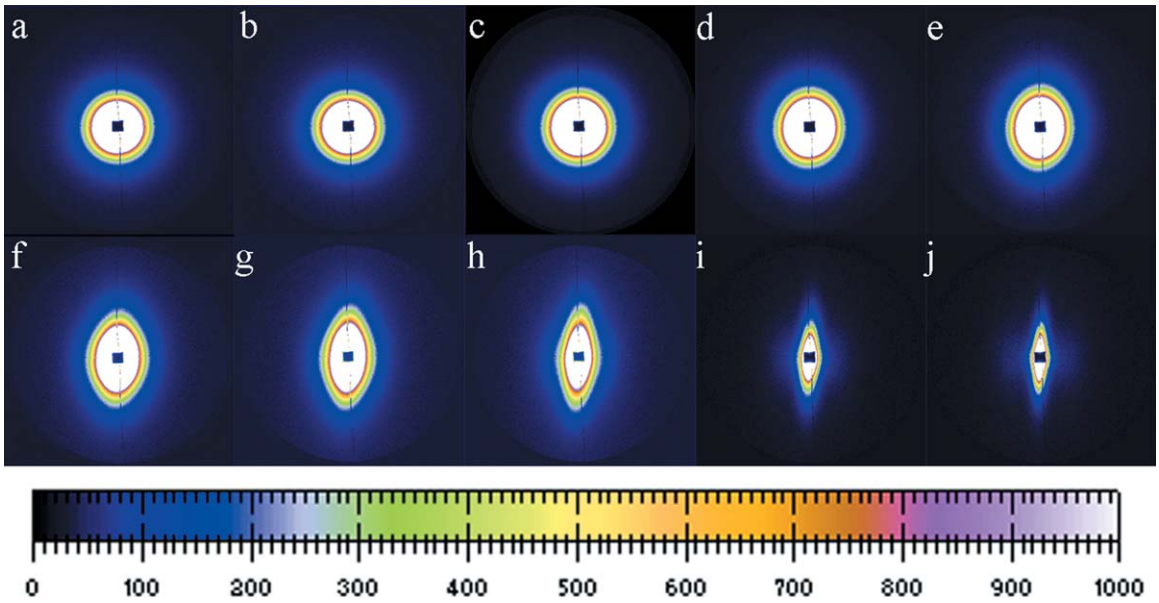

Figure 2. SAXS patterns of the pristine HDPE at different strains (stretching direction is horizontal): (a) 0, (b) 10%, (c) 20%, (d) 30%, (e) 41%, (f) 51%, (g) 62%, (h) 72%, (i) 84%, (j) 100%. [Color figure can be viewed in the online issue, which is available at wileyonlinelibrary.com.]

anisotropic scattering patterns having an elliptical scattering rings where the long axis is perpendicular to the stretching direction begin to be observed gradually, as seen in Figures 2(b,c) and 3(b,c). In the regions II and III, the SAXS patterns are all anisotropic, and the elliptical scattering rings are getting more and more clear with increasing strain, as shown in both Figure 2 from (d) to (j) and Figure 3 from (d) to (j). It is implied that the lamellar stacks change during deformation, and the tendency of this change is anisotropic. Besides, the tendency to form the elliptical scattering rings is smaller for the irradiated HDPE than the unirradiated one, indicating that the change of the lamellar stacks develops more difficultly in the irradiated HDPE.

To characterize the structural evolution during deformation, the SAXS integrated intensity curves along the equator and the meridian at different strains are obtained by FIT2D software. The intensity along the equator is acquired by the integration in the azimuthal angle range of $-15° \leq \varphi \leq 15°$, and the intensity along the meridian is acquired by the integration in the azimuthal angle range of $75° \leq \varphi \leq 105°$. Figures 4 and 5 give the SAXS intensity curves for the unirradiated HDPE at different

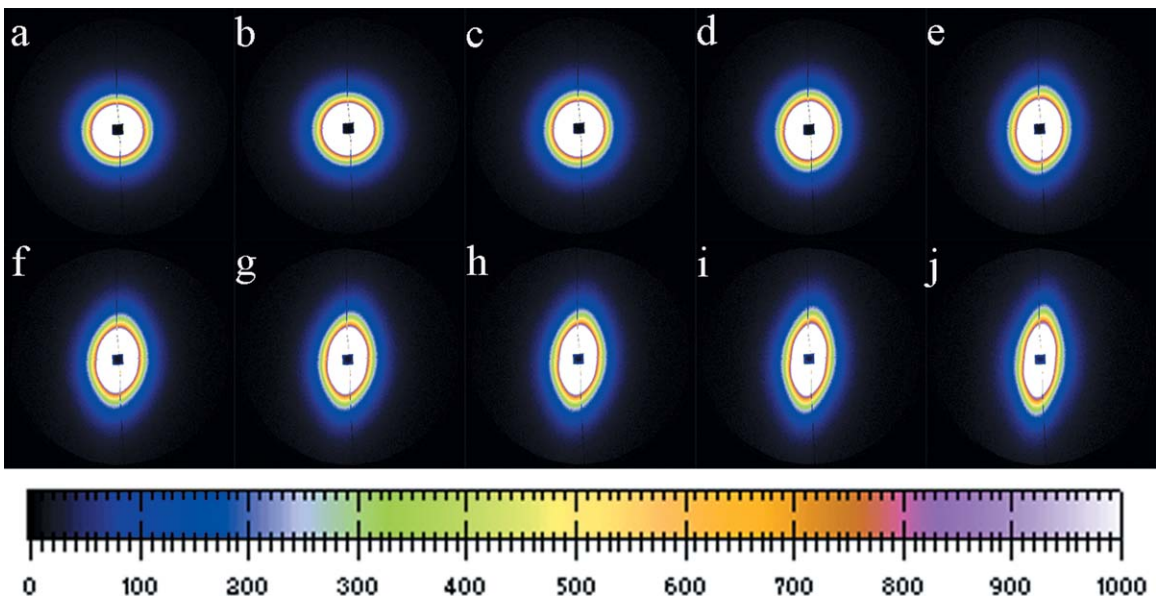

Figure 3. SAXS patterns of the irradiated HDPE at different strains (stretching direction is horizontal): (a) 0, (b) 10%, (c) 20%, (d) 30%, (e) 41%, (f) 51%, (g) 62%, (h) 72%, (i) 84%, (j) 100%. [Color figure can be viewed in the online issue, which is available at wileyonlinelibrary.com.]

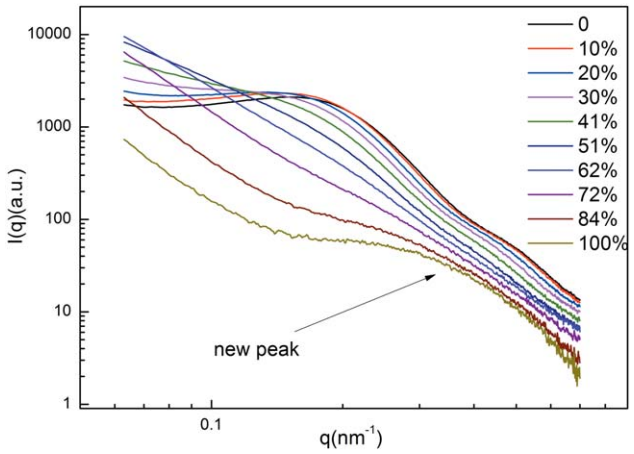

Figure 4. SAXS intensity curves of the pristine HDPE at different strains along the equator. [Color figure can be viewed in the online issue, which is available at wileyonlinelibrary.com.]

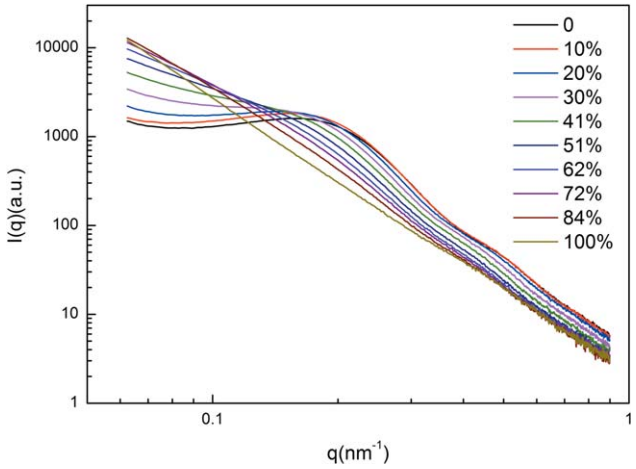

Figure 6. SAXS intensity curves of the irradiated HDPE at different strains along the equator. [Color figure can be viewed in the online issue, which is available at wileyonlinelibrary.com.]

strains along the equator and the meridian, respectively. Figures 6 and 7 show the SAXS intensity curves for the irradiated HDPE at different strains along the equator and the meridian, respectively. In these figures, q is the scattering vector ($q=4\pi \sin\theta/\lambda$, where θ is the scattering angle, λ is the wavelength of the incident X-ray), and $I(q)$ is the SAXS integrated intensity.

It is observed that the undeformed HDPE exhibits a distinct peak in the SAXS intensity plots for both the unirradiated and the irradiated one, and the peak position changes gradually from the strain of 0–20%, as shown in Figures 4–7. For the unirradiated HDPE, the peak becomes a weaker shoulder from the strain of 20–51%, and disappears from the strain of 51% for the scattering intensity along the equator (Figure 4). Similarly, the peak becomes a weaker shoulder from the strain of 20–72%, and disappears from the strain of 72% for the scattering intensity along the meridian (Figure 5). For the irradiated HDPE, the peak becomes a weaker shoulder from the strain of 20–72% and disappears from the strain of 72% for the scattering intensity along the equator (Figure 6). Also, the peak becomes a weaker shoulder from the strain of 20% and does not disappear even at the strain of 100% for the scattering intensity along the meridian (Figure 7). For the unirradiated HDPE, a new peak is prone to appear on the plot of scattering intensity along the equator from the strain of 84% (Figure 4). However, no new peaks appear even at the strain of 100% for the scattering intensity along the meridian (Figure 5). For the irradiated HDPE, no new peaks appear in the SAXS profiles even at the strain of 100% (Figures 6 and 7).

The intensity peak at a certain scattering vector q could be attributed to the lamellar structure of HDPE. In terms of the scattering vector q corresponding to the intensity peak, the long period L of the lamellar structure in HDPE can be calculated. Based on Bragg law ($2d\sin\theta=n\lambda$, where d is the long period in semicrystalline polymer, θ is the scattering angle, λ is the wavelength of the incident X-ray) and the definition of scattering vector q, the long period L, representing the average spacing

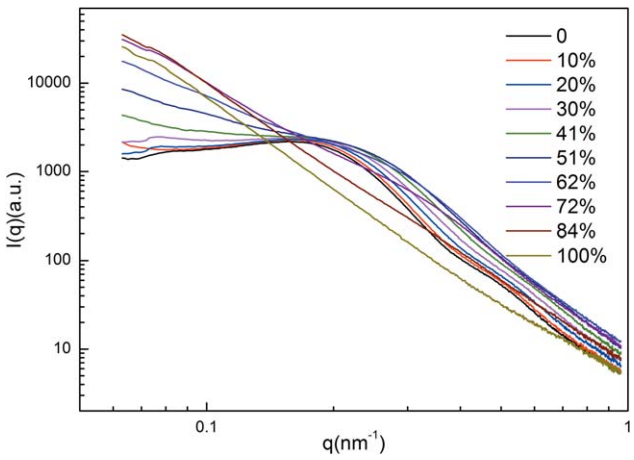

Figure 5. SAXS intensity curves of the pristine HDPE at different strains along the meridian. [Color figure can be viewed in the online issue, which is available at wileyonlinelibrary.com.]

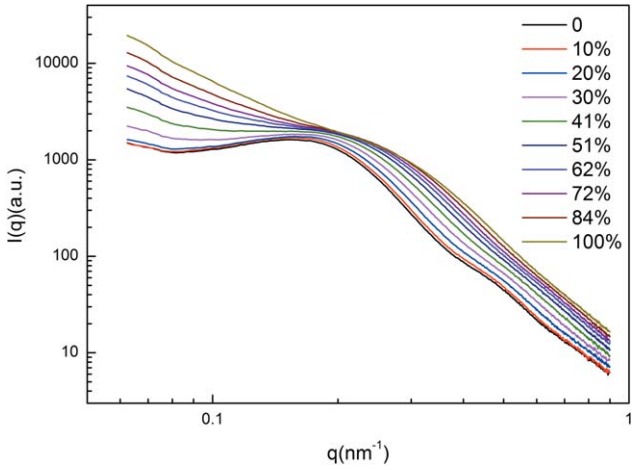

Figure 7. SAXS intensity curves of the irradiated HDPE at different strains along the meridian. [Color figure can be viewed in the online issue, which is available at wileyonlinelibrary.com.]

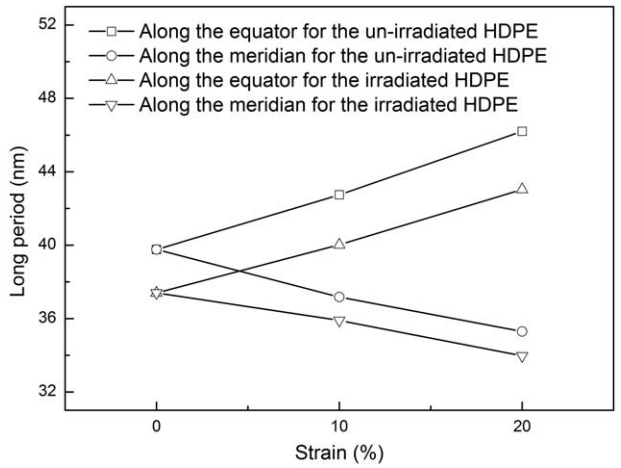

Figure 8. Long period as a function of strain for the unirradiated and the irradiated HDPE.

between adjacent crystalline lamellae, can be calculated by $L=2\pi/q_m$, where q_m is the scattering vector related to the peaks in SAXS intensity curves. The long periods along both the equator and the meridian are 39.8 nm for the undeformed pristine HDPE, and 37.4 nm for the undeformed irradiated HDPE, respectively. It is indicated that the crystalline lamellae are uniformly dispersed in the amorphous matrix, and the interlamellar spacing is constant in both the unirradiated and the irradiated HDPE. However, the irradiation decreases the long period of the HDPE.

In the region I, the appearance of elliptical scattering rings indicates that with increasing strain, the long period of the adjacent lamellae perpendicular to the stretching direction (corresponding to the scattering intensity along the equator) increases, while the long period of those parallel to the stretching direction (corresponding to the scattering intensity along the meridian) decreases, for both the unirradiated and the irradiated HDPE, as shown in Figure 8. The calculated results show that the long period of the adjacent lamellae perpendicular to the stretching direction increases from the initial 39.8–46.2 nm at the strain of 20% for the unirradiated HDPE, with a variation of 6.4 nm. In contrast, the long period of the adjacent lamellae parallel to the stretching direction decreases from the initial 39.8–35.3 nm at the strain of 20% for the unirradiated HDPE, with a variation of 4.5 nm. Similarly, the long period of the adjacent lamellae perpendicular to the stretching direction increases from the initial 37.4–43.6 nm at the strain of 20% for the irradiated HDPE, with a variation of 6.2 nm. Meanwhile, the long period of the adjacent lamellae parallel to the stretching direction decreases from the initial 37.4–33.1 nm at the strain of 20% for the irradiated HDPE, with a variation of 4.3 nm. The change in long period in Figure 8 verifies that the tensile deformation of the amorphous chains between lamellae dominates in the region I.

In the regions II and III, with increasing strain, the intensity peak gradually decays and even disappears, and forms again at higher strains. The decay of the intensity peak might indicate the disintegration of original lamellae, while the appearance of new peak is related to the formation of new crystals. The newly formed crystals possess different long period from the original lamellae, leading to a different peak position. In addition, it is easy to notice that the disintegration of original lamellae for the irradiated HDPE is slower than that for the pristine one, and new crystals form hardly in the irradiated HDPE and their formation is much slower than that for the pristine one.

The above results of SAXS analysis demonstrate that the deformation could be primarily related to the amorphous chains between lamellae in the region I, whereas the disintegration of original lamellae and the formation of new crystals occur in the regions II and III. These changes in the structure of HDPE are affected by irradiation and could be responsible for the deformation behavior and help to reveal the deformation mechanisms.

WAXD Analysis

Figures 9 and 10 give the *in situ* WAXD patterns during uniaxial tensile deformation for the unirradiated and the irradiated HDPE, respectively. For both the unirradiated and the irradiated HDPE, isotropic diffraction patterns are observed when the deformation is zero, as shown in Figures 9(a) and 10(a). With increasing strain in the region I, the scattering rings tend to change their shape from the circular to the elliptical gradually, as seen in Figures 9(b,c) and 10(b,c). In the regions II and III, the WAXD patterns are all anisotropic, as shown in both Figure 9 from (d) to (j) and Figure 10 from (d) to (j). It is revealed that the tendency to form elliptical scattering rings is smaller for the irradiated HDPE than that for the unirradiated one.

To characterize the structural evolution during deformation, the WAXD integrated intensity curves along the equator and the meridian at different strains are obtained by FIT2D software. The intensity along the equator is acquired by the integration in the azimuthal angle range of $-15^\circ \leq \varphi \leq 15^\circ$, and the intensity along the meridian is acquired by the integration in the azimuthal angle range of $75^\circ \leq \varphi \leq 105^\circ$. Figures 11 and 12 give the WAXD intensity curves of the unirradiated HDPE at different strains along the equator and the meridian, respectively. Figures 13 and 14 show the WAXD intensity curves of the irradiated HDPE at different strains along the equator and the meridian, respectively.

It is observed that there are two distinct peaks ((110) peak and (200) peak) in the WAXD intensity plots for both the unirradiated and the irradiated HDPE, and the peaks exist during the whole deformation process, as shown in Figures 11–14. The intensities of the (110) and (200) peaks change a little at the strains <20% for both the unirradiated and the irradiated HDPE. For the unirradiated HDPE, the intensities of the (110) and (200) peaks decrease from the strain of 20% for the scattering intensity along the equator (Figure 11). The intensity of the (110) peak decreases from the strain of 20%, while the intensity of the (200) peak increases from the strain of 20–72%, and decreases from the strain of 72% for the scattering intensity along the meridian (Figure 12). For the irradiated HDPE, the evolution of the intensities of the (110) and (200) peaks is similar as the unirradiated one (Figures 13 and 14). For the unirradiated HDPE, a new peak at about 17.2° appears at the strain

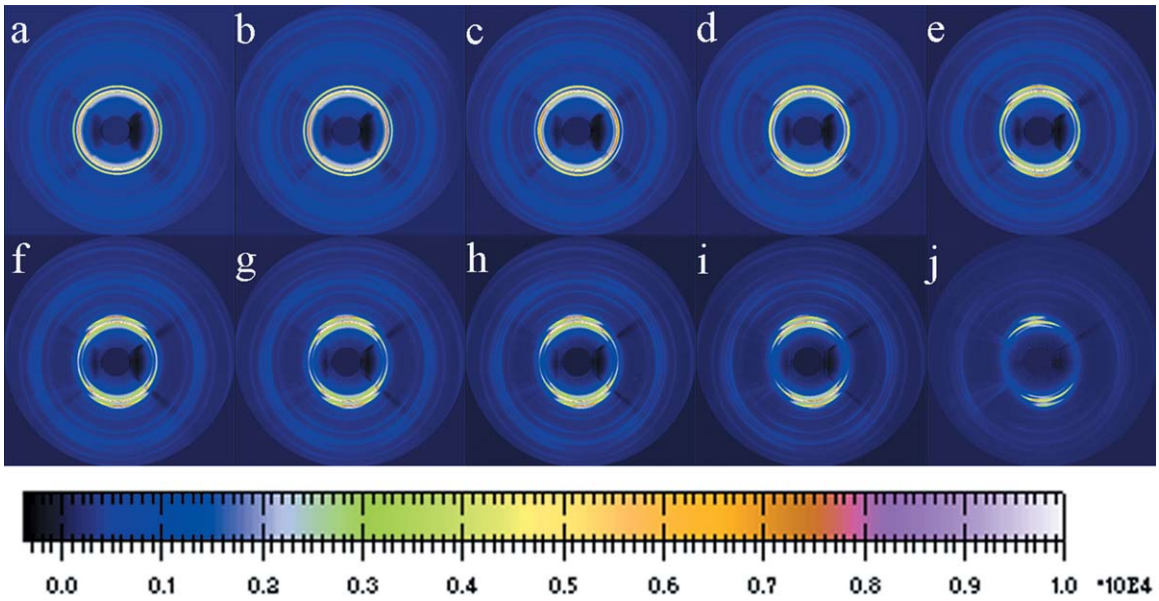

Figure 9. WAXD patterns of the pristine HDPE at different strains (stretching direction is horizontal): (a) 0, (b) 10%, (c) 20%, (d) 30%, (e) 41%, (f) 51%, (g) 62%, (h) 72%, (i) 84%, (j) 100%. [Color figure can be viewed in the online issue, which is available at wileyonlinelibrary.com.]

of 20%, and the intensity of this peak increases from the strain of 20–30%, and then decreases from the strain of 30% for the scattering intensity along the equator (Figure 11). Three new peaks at about 17.2°, 20.4°, and 22.2° appear at the strain of 20%, and the intensities of them increase from the strain of 20–72%, and then decrease from the strain of 72% for the scattering intensity along the meridian (Figure 12). For the irradiated HDPE, a new peak at about 17.2° appears at the strain of 20%, and the intensity of this peak increases from the strain of 20–30%, and then decreases from the strain of 30% for the scattering intensity along the equator (Figure 13). Three new peaks at about 17.2°, 20.4°, and 22.2° appear at the strain of 20%, and the intensities of them increase from the strain of 20% for the scattering intensity along the meridian (Figure 14).

The above results indicate that, in the region I, the intensities of the (110) and (200) peaks change a little at the strains <20% for both the unirradiated and the irradiated HDPE. It suggests that deformation could be primarily related to the amorphous chains between lamellae in the region I.

In the regions II and III, with further increasing strains from 20–100%, for both the unirradiated and the irradiated HDPE,

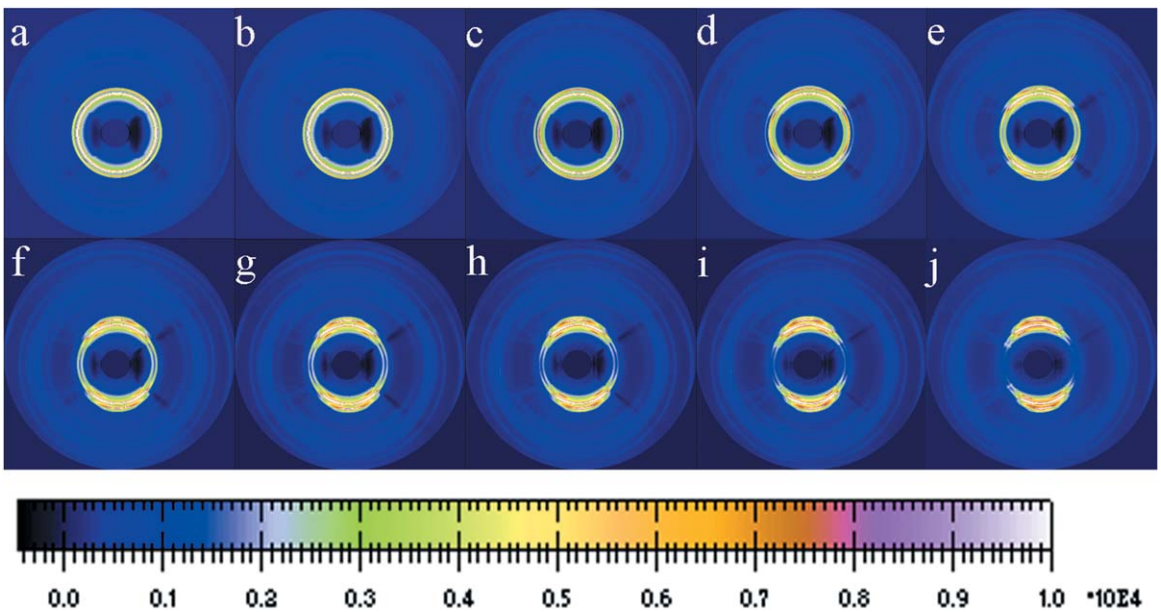

Figure 10. WAXD patterns of the irradiated HDPE at different strains (stretching direction is horizontal): (a) 0, (b) 10%, (c) 20%, (d) 30%, (e) 41%, (f) 51%, (g) 62%, (h) 72%, (i) 84%, (j) 100%. [Color figure can be viewed in the online issue, which is available at wileyonlinelibrary.com.]

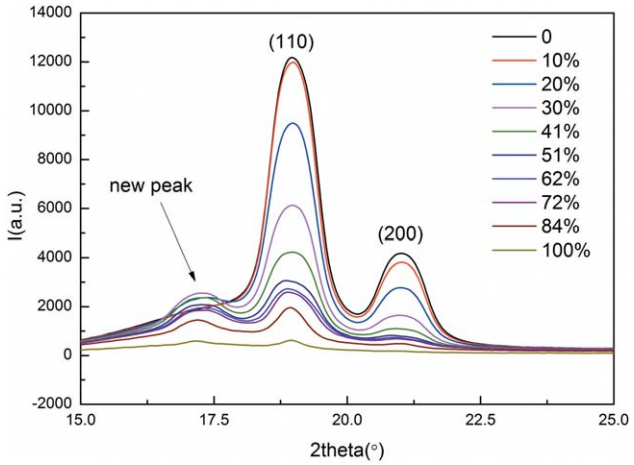

Figure 11. WAXD intensity curves of the pristine HDPE at different strains along the equator. [Color figure can be viewed in the online issue, which is available at wileyonlinelibrary.com.]

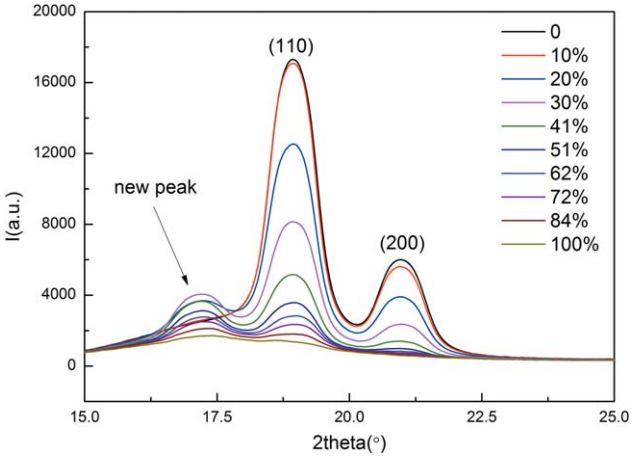

Figure 13. WAXD intensity curves of the irradiated HDPE at different strains along the equator. [Color figure can be viewed in the online issue, which is available at wileyonlinelibrary.com.]

the intensities of the (110) and (200) peaks change and new diffraction peaks appear at some diffraction angles. The intensity of the (110) and (200) diffraction peaks along the equator decreases during this stage, which indicates that the disintegration of the original crystals could occur. The intensity of the (110) peak along the meridian also decreases during this stage due to the disintegration of the original crystals. However, the intensity of the (200) peak along the meridian increases from the strain of 20–72% first, and then decreases from the strain of 72%. It indicates that the rotation of the disintegrated lamellae may occur. During tensile process, the disintegrated lamellae parallel to the stretching direction (corresponding to the diffraction intensity along the equator) rotate to be perpendicular to the stretching direction (corresponding to the diffraction intensity along the meridian). The rotation of the disintegrated lamellae from parallel to the stretching direction to perpendicular to the stretching direction leads to increasing the diffraction intensity along the meridian and decreasing the diffraction intensity along the equator. Because of the combined effect of the disintegration of the original crystals and the rotation of the disintegrated lamellae parallel to the stretching direction, the intensity of the (200) peak along the meridian increases from the strain of 20–72% first, and then decreases from the strain of 72%, while the intensity of the (200) peak along the equator decreases constantly. It is also found that the decrease of the intensity of (110) peak along the meridian is slower than that along the equator, which indicates that the evolution of the (110) peak is also affected by the combined effect of the disintegration of the original crystals and the rotation of the disintegrated lamellae parallel to the stretching direction. It is believed that the change of the new diffraction peaks might also be related to both the formation and the rotation of the new crystals. The new crystals may produce diffraction at about 17.2°, 20.4°, and 22.2°, leading to increasing the intensity of the new diffraction peaks during deformation. On the other hand, the rotation of the new crystals might decay the new diffraction peak. Because of the combined effect of the formation and rotation of the new crystals, the intensity of these new peaks

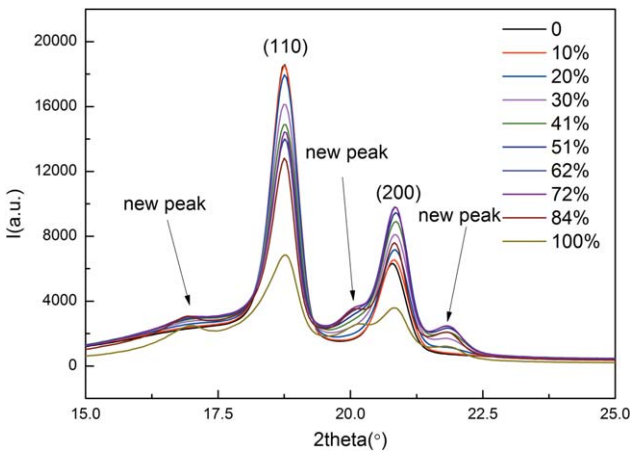

Figure 12. WAXD intensity curves of the pristine HDPE at different strains along the meridian. [Color figure can be viewed in the online issue, which is available at wileyonlinelibrary.com.]

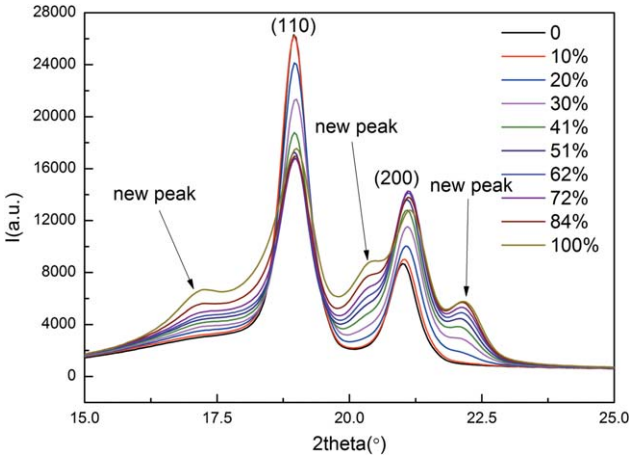

Figure 14. WAXD intensity curves of the irradiated HDPE at different strains along the meridian. [Color figure can be viewed in the online issue, which is available at wileyonlinelibrary.com.]

increases firstly and then decreases. Similar to rotation of the disintegrated lamellae, rotation of the new crystals is mainly from the lamellae parallel to the stretching direction (corresponding to the diffraction intensity along the equator) to that perpendicular to the stretching direction (corresponding to the diffraction intensity along the meridian). As a result of this, the intensity of these new peaks along the equator decreases from the strain of 30%, while that along the meridian decreases from the strain of 72% for the pristine sample and from the strain of more than 100% for the irradiated sample. Further, new peaks at about 20.4° and 22.2° appear along the meridian, but absent along the equator. Moreover, the peak width along the equator is significantly larger than that along the meridian (see Figures 11–14). From the above analyses, it can be concluded that the degree of crystallinity along the meridian is higher than that along the equator, and there is a preferred orientation along the meridian.

The above results of WAXD analysis demonstrate that the deformation could be primarily related to the amorphous chains between lamellae in the region I. Except the occurrence of the disintegration of original lamellae and the formation of new crystals in the regions II and III, the rotation of the disintegrated lamellae and the new crystals could also take place. Similarly as the above SAXS analysis, all these changes in the structure of HDPE are affected by irradiation and could be responsible for the deformation behavior and help to reveal the deformation mechanisms.

Deformation Mechanisms and Models

Based on the above results, the schematic diagrams of deformation models for the unirradiated and the irradiated HDPE can be shown in Figure 15. The models are proposed in two extreme orientations: (1) the stacking lamellae parallel to the stretching direction and (2) the stacking lamellae perpendicular to the stretching direction.

For the undeformed HDPE, it is noted that the 1 MeV electrons irradiation leads to decreasing the long period of the lamellar structure. Under the irradiation, free radicals could be generated on the molecular chains in the HDPE, which can react either with oxygen to cause chain scission or react internally to form crosslinking. Because of crosslinking, the average spacing between adjacent crystalline lamellae decreases.

In the region I, the change in long period can be related to deformation of the amorphous chains between stacking lamellae. Because the deformation of the amorphous chains proceeds under the constraint of the lamellae, strain-hardening takes place during the nonlinear deformation for the pristine sample and during the second linear deformation for the irradiated sample (both at the strains from 10 to 20%). During the deformation, the average spacing of the lamellae oriented parallel to the stretching direction is reduced, while that for the lamellae oriented perpendicularly to the stretching direction is increased. Crosslinking network forms in the amorphous matrix after irradiation and plays an important role in strengthening the HDPE.[32] Because of the crosslinking, the mobility of molecular chains for the irradiated HDPE is much lower than the unirradiated HDPE. The crosslinking sites could block the movement of chains, resulting in higher stress at a given strain. Accordingly, for the same long period change, the stress required for the irradiated HDPE is higher than that for the pristine one.

In the regions II and III, the disintegration of original lamellae occurs and new crystals are generated. The former process is referred to as the strain-induced melting,[33] and the latter as the strain-induced crystallization.[34] The strain-induced melting and strain-induced crystallization are used to separately describe the destruction and formation of some crystalline entities during deformation.[35] The strain-induced melting takes place at higher strains, where the stress in amorphous chains could exceed the crystal binding force, resulting in chain pullouts and disintegration of the lamellae.[33] Besides, the lamellae parallel to the stretching direction could rotate easier during deformation. The amorphous chains perpendicular to the stretching direction would have to be reoriented in the stretching direction. If the local stress concentration can overcome the crystal binding energy, the lamellae would not only be disintegrated into smaller blocks but also be rotated in order to alleviate the stress concentration.[33] The crystallization in the undeformed HDPE could be related to the folded-chain conformation, and the strain-induced crystallization is dominated by the extended-chain conformation. Strain-induced crystallization occurs at higher strains, for the extended-chain conformation is getting more and more.

It is found that the strain-induced melting and strain-induced crystallization proceed slower for the irradiated HDPE than the unirradiated HDPE. This can be explained as follows. The movement of molecular chains could be retarded by crosslinking sites, resulting in reduction of the possibility to form extended-chain conformation (strain-induced crystallization).[36] At larger strains, the local stress can be high enough to break the crosslinking sites in the irradiated HDPE. The break of crosslinking sites consumes a part of deformation energy and results in a decrease of local stress. Consequently, the chain pullouts and the disintegration of the lamellae (strain-induced crystallization) slow down.

In the regions II and III, the strain-induced melting and strain-induced crystallization exist simultaneously, for both the unirradiated and the irradiated HDPE. In the region II, the tensile stress decreases with strain (stain-softening), because the effect of strain-induced melting (the destruction of original crystals) dominates with respect to recrystallization (the formation of new crystals). In the region III, the original lamellae tend to be melted away, and the population of newly formed crystals increases with increasing strain. In the initial stage of region III, the synergistic effect of the melting and crystallization could result in tensile stress leveling off. With further increasing strain, the tensile stress increases again because the crystallization effect becomes dominant at larger strains. The newly formed crystals could produce a dispersion strengthening effect on the deformation of amorphous chains, leading to the secondary strain-hardening. Because of the effect of the irradiation-induced crosslinking network in the amorphous matrix, the tensile stress at a given strain is much higher for the irradiated HDPE than that for the pristine one.

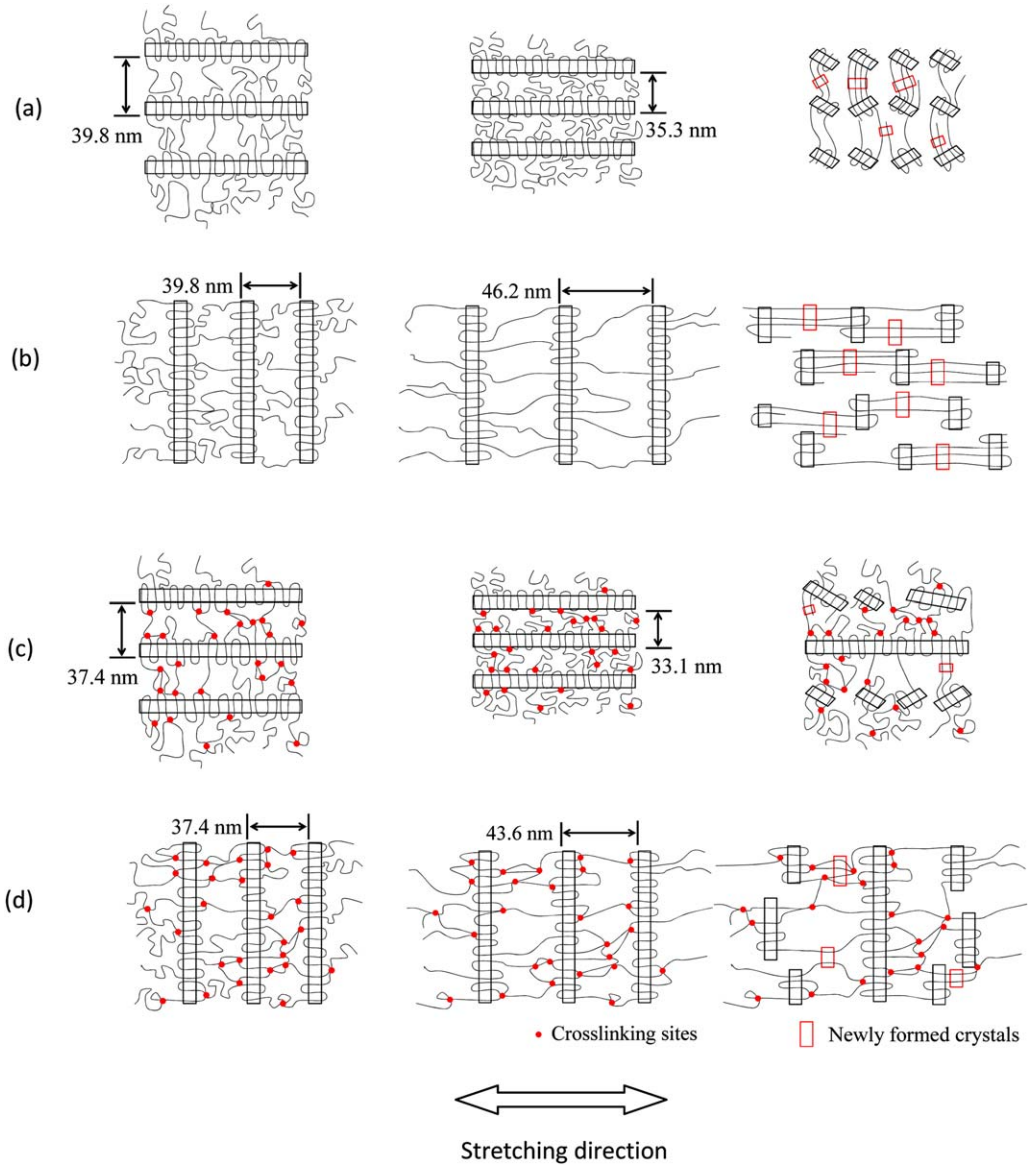

Figure 15. Schematic diagram of deformation models for the unirradiated and irradiated HDPE. (a) Lamellae arrayed parallel to the stretching direction for unirradiated HDPE. (b) Lamellae arrayed perpendicularly to the stretching direction for unirradiated HDPE. (c) Lamellae arrayed parallel to the stretching direction for irradiated HDPE. (d) Lamellae arrayed perpendicularly to the stretching direction for irradiated HDPE. [Color figure can be viewed in the online issue, which is available at wileyonlinelibrary.com.]

CONCLUSION

It is of significance to characterize the structure evolution during uniaxial tensile deformation of HDPE before and after irradiation by 1 MeV electrons for its space application. It is shown that both the pristine and the irradiated HDPE exhibit three stages of deformation behavior. In the region I, elastic deformation followed by yielding can be related to the amorphous chains, and strain-hardening occurs. With increasing strains from 20 to 72% (region II), the strain-induced melting and strain-induced crystallization could occur, and the melting of the original lamellae dominates, leading to decreasing the tensile stress with strain (strain-softening). In the region III, ranging from the strain higher than 72%, the original lamellae tend to be melted away, and the population of newly formed crystals increases with increasing strain. Because of the synergistic effect of melting and crystallization, the tensile stress could be leveling off, and then increases when the crystallization effect becomes dominant. Compared to the pristine one, the tensile stress at a given strain is much higher for the irradiated HDPE, due to the formation of irradiation-induced crosslinking network in the amorphous matrix.

ACKNOWLEDGMENTS

Erming Rui and Xingji Li mainly contributed to the experimental design and data analysis. Erming Rui, Jianqun Yang, Chaoming Liu, Feng Tian, and Xiuhong Li mainly contributed to the SAXS and WAXD tests. Feng Gao and Hongbin Geng mainly contributed to the materials preparation and manufacture of auxiliary devices.

The National Center for Nanoscience and Technology of China and Shanghai Synchrotron Radiation Facility is thanked for support of this work.

REFERENCES

1. Willis, P. B.; Hsieh, C.-H. *Kobunshi* **2000**, *49*, 52.
2. Bourdarie, S.; Xapsos, M. *IEEE Trans. Nucl. Sci.* **2008**, *55*, 1810.
3. Marenny, A. M.; Nymmik, R. A.; Tolstaya, E. D.; Benton, E. V. *Radiat. Meas.* **1996**, *26*, 493.
4. Baxter, R. M.; MacDonald, D. W.; Kurtz, S. M.; Steinbeck, M. J. *J. Biomed. Mater. Res. B* **2013**, *101B*, 467.
5. Tawab, K. A.; Ibrahim, S. M.; Magida, M. M. *J. Radioanal. Nucl. Chem.* **2013**, *295*, 1313.
6. Zhang, L.; Zhou, Y. X.; Huang, J. W.; Tian, J. H.; Wang, Y. S.; Sha, Y. C.; Huang, M. *J. Electrostat.* **2013**, *71*, 403.
7. Abdul-Kader, A. M. *J. Nucl. Mater.* **2013**, *435*, 231.
8. Furuta, M.; Hosoda, S.; Kojima, K. *J. Appl. Polym. Sci.* **1987**, *33*, 401.
9. Briscoe, B. J.; Pelillo, E.; Sinha, S. K. *Polym. Eng. Sci.* **1996**, *36*, 2996.
10. Adams, W. W.; Yang, D.; Thomas, E. L. *J. Mater. Sci.* **1986**, *21*, 2239.
11. Vanhutten, P. F.; Koning, C. E.; Pennings, A. J. *J. Mater. Sci.* **1985**, *20*, 1556.
12. Hillmansen, S.; Hobeika, S.; Haward, R. N.; Leevers, P. S. *Polym. Eng. Sci.* **2000**, *40*, 481.
13. Serban, D. A.; Weber, G.; Marsavina, L.; Silberschmidt, V. V.; Hufenbach, W. *Polym. Test.* **2013**, *32*, 413.
14. Bartczak, Z.; Beris, P. F. M.; Wasilewski, K.; Galeski, A.; Lemstra, P. J. *J. Appl. Polym. Sci.* **2012**, *125*, 4155.
15. Lu, Y.; Shinozaki, D. M.; Herbert, S. *J. Appl. Polym. Sci.* **2002**, *86*, 43.
16. Xiong, L.; Xiong, D. S.; Yang, Y. Y.; Jin, J. B. *Nucl. Instrum. Methods Phys. Res., Sect. B* **2010**, *268*, 2846.
17. Pruitt, L. A. *Biomaterials* **2005**, *26*, 905.
18. Clements, J.; Zachmann, H. G.; Ward, I. M. *Polymer* **1988**, *29*, 1929.
19. Song, H. H.; Stein, R. S.; Wu, D. Q.; Ree, M.; Phillips, J. C.; Legrand, A.; Chu, B. *Macromolecules* **1988**, *21*, 1180.
20. Wilke, W.; Bratrich, M. *J. Appl. Crystallogr.* **1991**, *24*, 645.
21. Bartczak, Z.; Argon, A. S.; Cohen, R. E. *Macromolecules* **1992**, *25*, 5036.
22. Vickers, M. E.; Fischer, H. *Polymer* **1995**, *36*, 2667.
23. Butler, M. F.; Donald, A. M.; Bras, W.; Mant, G. R.; Derbyshire, G. E.; Ryan, A. *J. Macromolecules* **1995**, *28*, 6383.
24. Tang, Y. J.; Jiang, Z. Y.; Men, Y. F.; An, L. J.; Enderle, H. F.; Lilge, D.; Roth, S. V.; Gehrke, R.; Rieger, J. *Polymer* **2007**, *48*, 5125.
25. Butler, M. F.; Donald, A. M.; Ryan, A. *J. Polymer* **1998**, *39*, 781.
26. Butler, M. F.; Donald, A. M.; Ryan, A. *J. Polymer* **1998**, *39*, 39.
27. Butler, M. F.; Donald, A. M.; Ryan, A. *J. Polymer* **1997**, *38*, 5521.
28. Butler, M. F.; Donald, A. M. *Macromolecules* **1998**, *31*, 6234.
29. Hughes, D. J.; Mahendrasingam, A.; Oatway, W. B.; Heeley, E. L.; Martin, C.; Fuller, W. *Polymer* **1997**, *38*, 6427.
30. Butler, M. F.; Donald, A. M. *J. Appl. Polym. Sci.* **1998**, *67*, 321.
31. Kamal, T.; Shin, T. J.; Park, S. Y. *Macromolecules* **2012**, *45*, 8752.
32. Murray, K. A.; Kennedy, J. E.; McEvoy, B.; Vrain, O.; Ryan, D.; Cowman, R.; Higginbotham, C. L. *Nucl. Instrum. Methods Phys. Res., Sect. B* **2013**, *297*, 64.
33. Liu, L. Z.; Hsiao, B. S.; Fu, B. X.; Ran, S. F.; Toki, S.; Chu, B.; Tsou, A. H.; Agarwal, P. K. *Macromolecules* **2003**, *36*, 1920.
34. Martins, C. I.; Cakmak, M. *Polymer* **2007**, *48*, 2109.
35. Tsubakihara, S.; Yasuniwa, M. *Polym. J. (Tokyo, Jpn.)* **1996**, *28*, 563.
36. Mchugh, A. J.; Yung, W. S. *J. Polym. Sci. B Polym. Phys.* **1989**, *27*, 431.